



**HAL**  
open science

# Spin-polarized resonant surface state in $(1\ 1\ 1)$ $\text{Sm}_{1-x}\text{Gd}_x\text{Al}_2$ , a zero- magnetization ferromagnet

Mathias Bersweiler, Karine Dumesnil, Yannick Fagot-Revurat, Patrick Le Fèvre, Coriolan Tiusan, Daniel Lacour, Michel Hehn

► **To cite this version:**

Mathias Bersweiler, Karine Dumesnil, Yannick Fagot-Revurat, Patrick Le Fèvre, Coriolan Tiusan, et al.. Spin-polarized resonant surface state in  $(1\ 1\ 1)$   $\text{Sm}_{1-x}\text{Gd}_x\text{Al}_2$ , a zero- magnetization ferromagnet. *Journal of Physics: Condensed Matter*, 2018, 30 (43), pp.435501. 10.1088/1361-648X/aae341 . hal-02949091

**HAL Id: hal-02949091**

**<https://hal.science/hal-02949091>**

Submitted on 24 Mar 2024

**HAL** is a multi-disciplinary open access archive for the deposit and dissemination of scientific research documents, whether they are published or not. The documents may come from teaching and research institutions in France or abroad, or from public or private research centers.

L'archive ouverte pluridisciplinaire **HAL**, est destinée au dépôt et à la diffusion de documents scientifiques de niveau recherche, publiés ou non, émanant des établissements d'enseignement et de recherche français ou étrangers, des laboratoires publics ou privés.

ACCEPTED MANUSCRIPT

## Spin-polarized resonant surface state in (111) $\text{Sm}_{1-x}\text{Gd}_x\text{Al}_2$ , a zero-magnetization ferromagnet

To cite this article before publication: Mathias Bersweiler *et al* 2018 *J. Phys.: Condens. Matter* in press <https://doi.org/10.1088/1361-648X/aae341>

### Manuscript version: Accepted Manuscript

Accepted Manuscript is “the version of the article accepted for publication including all changes made as a result of the peer review process, and which may also include the addition to the article by IOP Publishing of a header, an article ID, a cover sheet and/or an ‘Accepted Manuscript’ watermark, but excluding any other editing, typesetting or other changes made by IOP Publishing and/or its licensors”

This Accepted Manuscript is © 2018 IOP Publishing Ltd.

During the embargo period (the 12 month period from the publication of the Version of Record of this article), the Accepted Manuscript is fully protected by copyright and cannot be reused or reposted elsewhere.

As the Version of Record of this article is going to be / has been published on a subscription basis, this Accepted Manuscript is available for reuse under a CC BY-NC-ND 3.0 licence after the 12 month embargo period.

After the embargo period, everyone is permitted to use copy and redistribute this article for non-commercial purposes only, provided that they adhere to all the terms of the licence <https://creativecommons.org/licenses/by-nc-nd/3.0>

Although reasonable endeavours have been taken to obtain all necessary permissions from third parties to include their copyrighted content within this article, their full citation and copyright line may not be present in this Accepted Manuscript version. Before using any content from this article, please refer to the Version of Record on IOPscience once published for full citation and copyright details, as permissions will likely be required. All third party content is fully copyright protected, unless specifically stated otherwise in the figure caption in the Version of Record.

View the [article online](#) for updates and enhancements.

# Spin-polarized resonant surface state in (111) $\text{Sm}_{1-x}\text{Gd}_x\text{Al}_2$ , a zero-magnetization ferromagnet

M. Bersweiler<sup>1</sup>, K. Dumesnil<sup>1</sup>, Y. Fagot-Revurat<sup>1</sup>, P. Le Fèvre<sup>2</sup>, C. Tiusan<sup>3</sup>, D. Lacour<sup>1</sup> and M. Hehn<sup>1</sup>

<sup>1</sup>*Institut Jean Lamour (UMR CNRS 7198), Université de Lorraine, 54000 Nancy, France*

<sup>2</sup>*Synchrotron SOLEIL, L'Orme des Merisiers, 91192 Gif-sur Yvette, France*

<sup>3</sup>*Center for Superconductivity, Spintronics and Surface Science, Technical University of Cluj-Napoca, 400114 Cluj-Napoca, Romania*

## Abstract

The electronic structure of (111)  $\text{Sm}_{1-x}\text{Gd}_x\text{Al}_2$ , a zero-magnetization ferromagnet, is investigated by angle- and spin-resolved photoemission spectroscopy. An intense electron pocket strongly localized around  $\bar{\Gamma}$  and close to the Fermi level is observed and analyzed in detail. Its various characteristics, combined with electronic structure calculations, reveal a resonant surface state of  $5d$  character and  $\Lambda_1$  symmetry, likely built on bulk states developing around L points. It exhibits moreover a low temperature positive spin polarization at the Fermi level, of strong interest for spin-dependent transport properties in  $\text{Sm}_{1-x}\text{Gd}_x\text{Al}_2$ -based spintronic devices.

E-mail: karine.dumesnil@univ-lorraine.fr

## 1. Introduction

Surfaces and interfaces are peculiar regions in a material because of the reduced number of neighboring atoms compared to the bulk and the consequent symmetry breaking. This may give rise to specific magnetic or electronic surface properties. The number of surface atoms is often negligible compared to those in the bulk, but these cannot be ignored (*i*) when considering any exchange between the material and the outside (*ii*) when dealing with thin films and nanosystems where the surface to bulk ratio greatly increases. In this latter case, electronic and magnetic surface/interface properties have shown to be especially critical for the understanding of spin-dependent transport in spintronic devices, such as spin valves [1], magnetic tunnel junctions (MTJs) [2–5] and spin-orbit torque based systems [6]. The Fe(001) surface states are for instance responsible for specific features in the spin-dependent transport across the interface with GaAs: tunneling anisotropic magnetoresistance or variation of tunneling current spin polarization with applied bias [4]. An intense research activity is thus focused on electronic surface/interface properties of conventional magnetic  $3d$  transition materials but also of some challenging strategic materials for spintronics such as Heusler alloys [7] or topological insulators [8].

Among unconventional strategic materials for spintronics, the Rare Earth (RE) dialuminide  $\text{Sm}_{1-x}\text{Gd}_x\text{Al}_2$  (SGA) exhibits very peculiar and original magnetic properties. It can be considered as a zero-magnetization ferromagnetic material, as it has been proved first in bulk by various techniques [9–15]. Because the spin and orbital magnetic contributions are antiparallel and exhibit different temperature dependences, there exists a so-called compensation temperature, where the compound exhibits a long range ferromagnetic order of spin contributions, together with a zero magnetization. This characteristic makes SGA an original compound with rich properties, as it has been explored by several authors around the compensation point [16–18]. It is especially well suited for use in spintronic devices since, despite a uniform spin polarization, it doesn't perturb the motion of charged particles due to the absence of stray magnetic fields. Zero-magnetization spin-polarized electrodes for MTJs are also very attractive since magnetic dipolar coupling issues from the reference electrode should be eliminated when scaling down device size. This motivates researches on SGA thin films' growth and magnetic/electronic properties. The successful growth of high quality epitaxial SGA films [19,20]

permitted to confirm the zero-magnetization ferromagnetic character in these low dimension systems [21,22] and to eventually build SGA-based MTJ's [23,24]. Their transport properties however ultimately depend on the spin polarization and on the electronic states of the SGA/insulator interface, which remain largely unknown. Although Laubschat *et al.* investigated RE-Al<sub>2</sub> electronic properties thirty years ago [25], they mainly analyzed the stability of the RE 4*f* configurations, and except for a recent 3D Angle Resolved PhotoEmission Spectroscopy (ARPES) study of YbAl<sub>2</sub> [26], the RE-Al<sub>2</sub> band structure has been up to now exclusively described via electronic band structure calculations [27–31].

The present study aims to investigate the electronic surface properties of (111) SGA epitaxial thin films and to contribute to a better understanding of surface/interface electronic properties in strategic materials for spintronics application. In this paper, we report on the first results of synchrotron based 3D-ARPES and Spin Resolved PES (SRPES) performed on a (111) SGA epitaxial film. Several dispersive electronic states are observed despite the occurrence of relatively intense Sm 4*f* divalent multiplets. An electron pocket, close to the Fermi level and strongly localized around the  $\bar{\Gamma}$  point is especially analyzed. Its various characteristics reveal a spin-polarized resonant surface state, likely built on bulk states, as this is supported by electronic structure calculations. The occurrence of such a spin-polarized resonant surface state is highly relevant for spin-dependent transport properties in SGA-based spintronics devices, as this has been highlighted in other magnetic materials.

## 2. Experimental details

A 300nm-thick (111) Sm<sub>0.975</sub>Gd<sub>0.025</sub>Al<sub>2</sub> epitaxial film was first grown by MBE [22] at the Institut Jean Lamour (IJL) laboratory in Nancy. The co-deposition of Sm, Gd and Al atoms was performed at 510°C on a (110) Nb buffer covering a (11 $\bar{2}$ 0)sapphire substrate. A 25 nm thick Nb capping layer was then deposited at room temperature to protect the compound from oxidization in air. The structural and magnetic properties have been described in previous studies on (111) SGA thin films, in particular the giant coercive field exceeding 7T below the compensation temperature (88K in this film) [22,32].

The surface preparation, ARPES and SRPES measurements were carried out on the CASSIOPEE beamline setup at the SOLEIL synchrotron. The surface preparation of PES samples is a crucial step for such surface sensitive analysis. A two-steps specific preparation process has been developed in the CASSIOPEE MBE chamber to recover a high quality (111) SGA surface. First, *the Nb cover layer is removed by Ar sputter etching*; RHEED analysis confirmed that the (111) SGA crystal order is preserved after the etching process. The second step is the *annealing of the SGA surface*; a “flash heating” at high temperature (above 550°C during 15 min) desorbs residual impurities, rearranges and smooths the surface, as attested by more continuous RHEED streaks. XPS measurements of the Al 2*p* contributions confirmed that, for optimal preparation conditions, only the 2*p*<sub>1/2</sub> and 2*p*<sub>3/2</sub> lines of metallic Al are observed, separated by a spin-orbit coupling of 0.4eV. The process of fast etching and annealing has been repeated before each ARPES acquisition in order to recover the initial quality of the SGA surface which is naturally unstable, due to the high affinity of Sm and Al to oxygen. It was nevertheless stable enough for 4-5 hours ARPES measurements.

Electronic properties have been explored along different directions of the (111) SGA Surface Brillouin Zone (SBZ) and of the bulk Brillouin Zone. High symmetry directions of the SBZ are ( $\bar{\Gamma}\bar{K}$ ) and ( $\bar{\Gamma}\bar{M}$ ) with  $|\bar{\Gamma}\bar{K}| = 0.74 \text{ \AA}^{-1}$  and  $|\bar{\Gamma}\bar{M}| = 0.64 \text{ \AA}^{-1}$ . More details about the (111) SBZ of fcc lattice can be found in reference [33].

## 3. Experimental results

The ARPES results obtained at 5K along  $\bar{\Gamma}\bar{K}$  and  $\bar{\Gamma}\bar{M}$ , for an incident photon energy of 32 eV and p-polarization, are presented in **figure 1** (raw data on the left). In addition to several dispersive contributions, discussed in the following, two non-dispersive contributions, localized around -0.6 eV and -1.6 eV, are observed for both directions. Their positions relative to the Fermi level, as well as complementary resonant photoemission experiments, permit us to identify these as Sm 4*f* divalent multiplets, <sup>6</sup>H and <sup>6</sup>F respectively. These have been previously observed for Sm metal and several Sm-based compounds, including SmAl<sub>2</sub>, and are attributed to the occurrence of divalent Sm atoms at surfaces [34–36]. To emphasize the other dispersive contributions, each energy dispersion curve (EDC) in the ARPES image was normalized to the angle-integrated spectrum, as proposed by Matsunami *et al.* [26]. The resulting maps are shown in **figure 1** (right part). Three main features are then observed along both directions:

① an intense electron pocket, close to the Fermi level and strongly localized around the  $\bar{\Gamma}$  point, ② two downwards dispersive bands observed for binding energies up to -0.8 eV, and ③ one dispersive band for larger binding energies with a minimum around -3 eV.

From in-plane dispersion curves (**figure 2a**) obtained by fitting the Momentum Dispersion Curves (MDC) and adjusted using the nearly-free electron model approximation, we extract the effective mass  $m^*$  for the different dispersive contributions. The fitted values of  $m^*$  and the binding energy at the  $\bar{\Gamma}$  point ( $E_0$ ) are reported on the side of the curves. The electron pocket ① and the electronic band ③ have similar positive  $m^*/m_e$  ratio which may suggest a similar origin. The contributions ② present a slightly larger negative  $m^*/m_e$  ratio related to the downwards energy dispersion. Iso-energy ( $k_x, k_y$ ) maps for increasing binding energies across the electron pocket ① (**figure 2b**) clearly reveal in-plane isotropic properties, with the occurrence of a well-defined ring around the  $\bar{\Gamma}$  point of the SBZ. This shape of a paraboloid of revolution is similarly observed for other contributions ② and ③ (**figure 2(c)**). It points out similar effective masses along  $k_x$  and  $k_y$ , and the localization of these electronic states far from zone boundaries.

The dependence on the perpendicular component of the momentum  $k_z$  was explored by varying the incident photon energy. It appears that the various contributions exhibit reasonable spectral weight only in a very narrow energy range (approx. 30-39 eV) with a strong dependence on the photon energy and a maximum around 34 eV. This makes the analysis difficult since the available range to determine the inner potential  $V_0$  and to calculate  $k_z$  is limited.  $V_0$  is known to be comprised between 11eV and 15eV, a value of 13.7eV being reported for YbAl<sub>2</sub> [26]. Whatever the inner potential in this possible 11eV-15eV range, the variation of binding energy is extremely weak, approximately 125meV/Å<sup>-1</sup>, i.e. 10 times smaller than what is measured in the ( $k_x, k_y$ ) plane.

A value of  $V_0 = 15$  eV, in reasonable agreement with previous reports for dialuminides [26], is used to compare Fermi surface mapping in the ( $k_z, k_y$ ) and in the ( $k_x, k_y$ ) planes (**figure 3**). For this  $V_0$  value, the maximum intensity (at 34eV) occurs around a L point in the fifth BZ ( $k_z = 5|\bar{\Gamma}L| = 3.425 \text{ \AA}^{-1}$ ). Vertical straight features are visible at  $k_y = \pm 0.09 \text{ \AA}^{-1}$  in the ( $k_z, k_y$ ) plane (**figure 3b**), in contrast with the ring observed in the ( $k_x, k_y$ ) plane (**figure 3c**). Additional experiments with higher photon energy could be envisioned to explore another BZ and to analyse further the dispersion along the  $k_z$  direction, but this first result is already a strong indication of the two dimensional character of this electronic state.

The symmetry of this 2D state is investigated by varying the incident photon beam polarization (*s*- or *p*-type). For *s*-polarization, the electric field is perpendicular to the incidence plane, i.e. parallel to the sample surface. For *p*-polarization, the electric field is in the incidence plane. EDC curves measured at the  $\bar{\Gamma}$  point for both *p*- and *s*-polarizations are presented in **figure 4a** after subtraction of the divalent contributions. The contributions close to the Fermi level and for binding energies above -2.5 eV obviously vanish when switching to *s*-polarization. The remaining spectral weight in the vicinity of -0.6 eV and -1.6 eV is likely due to residual divalent parts, not fully subtracted as it is also seen for the *p*-polarization. As a result of the optical transitions for the photoelectron governed by Fermi's golden rules, only the initial states with the same symmetries as the electromagnetic field  $E$  can be excited in photoemission. Following the development proposed by J. Hermanson [37] for cubic crystals, the dipole-allowed initial symmetries for a (111) crystal face and for normal emission are either  $\Lambda_1$  (for electric field parallel to  $\langle 111 \rangle$ ) or  $\Lambda_3$  (for electric field in the (111) plane). One can therefore conclude that both ① and ② contributions identified in **figure 1** exhibit  $\Lambda_1$  symmetry.

Spin-Resolved photoemission spectroscopy measurements have been performed at 30K in the magnetic remanent state. For this purpose, we used a hemispherical analyzer SCIENTA SES 2002 coupled to a Mott detector for the spin analysis through a horizontal slit with an acceptance angle of  $\pm 8^\circ$  without angular resolution. In order to get rid of possible differences between detectors, measurements have been collected for two opposite orientations of the sample magnetization. Because of the huge coercivity observed in SGA films [32], the magnetization cannot be reversed in switching the magnetic field at low temperature. The two opposite magnetization states have thus been prepared in successively field-cooling the sample from above Curie temperature under +1200 Oe and then -1200 Oe (maximum field applied in the experimental setup). A positive polarization of approximately 13% (**figure 4b**) has been extracted in the vicinity of the Fermi energy, i.e. in the energy range corresponding to the above-mentioned electron pocket.

#### 4. Discussion-calculation

Experimental observations from the localized states close to the Fermi level are typical for surface states developing at the (111) surface, for example in noble metals [38,39]. It especially exhibits very limited dispersion along  $k_z$  compared to isotropic parabolic dispersion sheets in the surface plane. Moreover, we have observed that this state is strongly affected by the surface preparation and by the surface quality/contamination. The peak amplitude of the electron pocket, as well as of the divalent contributions, indeed strongly decreases in time (reduction by a factor of approximately 6 after 12 hours), likely due to some surface contamination despite the low base pressure (in the  $10^{-10}$  mbar range) inside the photoemission chamber. This proves that the divalent contributions and the electron pocket exhibit similar behavior and are both very sensitive to the surface.

The combination of these points strongly suggests the presence of an electronic resonant surface state. The maximum intensity measured for incident photon energy close to 34 eV is by the way consistent with a  $d$ -character, as expected from a  $5p \rightarrow 5d$  resonant process enhancing  $5d$  emission [40].

The occurrence of a surface state is a common property of lanthanide metal surfaces and has been observed for Gd [41,42], Lu [43], La [43], Tb [44], Tm [45], Yb [45], Sm [46]. To our knowledge, no surface state has however been reported up to now for SmAl<sub>2</sub> or more generally for RE-Al<sub>2</sub> compounds. For polycrystalline RE-Al<sub>2</sub>, C. Laubschat *et al.* [13] only identified divalent contributions as surface features and didn't observe any additional contribution at the Fermi level, certainly due to the higher incident photon energies (70-75 eV).

In order to strengthen our experimental results and analysis, electronic band structure calculations have been undertaken. Following the approach developed by H.J. Gotsis *et al.* [31], the Local Spin-Density Approximation (LSDA) incorporating the Hubbard parameter and the spin-orbit coupling (LSDA+U+SO) has been chosen, in order to properly locate the occupied and unoccupied  $4f$  states. The Wien2k code, based on the Full Potential Linearized Augmented Plane Waves (FP-LAPW) method, was used. Calculations have been first performed with a bulk cell crystallizing in the  $Fd\bar{3}m$  symmetry space group and with lattice constants equal to 7.912 Å. The Hubbard (U) parameter and the spin-orbit (SO) coupling have been chosen to get proper localization of the  $4f$  trivalent contributions compared to the experiment and satisfactory values for spin and orbital moments ( $m_{\text{orb}} = -3.23 \mu_B$  and  $m_{\text{spin}} = 2.95 \mu_B$ ). The calculated electronic band structure for bulk SmAl<sub>2</sub> is presented in **figure 5a** along WLK directions of the bulk Brillouin Zone. Note that the  $4f$  Sm<sup>3+</sup> bulk contributions do not appear in **figure 5a** since they are located out of the energy range, at approximately -7eV and slightly above 1eV. Moreover, this calculation performed using a bulk cell cannot describe the surface Sm<sup>2+</sup>  $4f$  divalent multiplets (<sup>6</sup>H and <sup>6</sup>F contributions).

The calculated electronic band structure can be compared to experimental data since the LK and LW bulk directions are probed via in-plane measurements along  $k_x$  and  $k_y$  respectively. Several features appear to be in good qualitative agreement with experimental observations around the bulk L point, i.e. the surface  $\bar{\Gamma}$  point (**figure 1**):

(i) two close dispersive bands (purple/orange) with positive effective mass appear with a bottom energy at approximately -3.2 eV, similar to the contribution ③ in **figure 1** (ii) two dispersive bands (pink/green) with negative effective mass appear with minimum binding energies around -0.4 eV and -0.2 eV, similar to the contribution ② in **figure 1** (iii) a contribution with positive effective mass (red) appears close to the Fermi level with a minimum around -0.1 eV, similar to the contribution ① in **figure 1**.

Calculations have been then extended to a different supercell with a tetragonal symmetry to simultaneously simulate the three possible environments for Sm: in the bulk of the layer, at the surface, or below the surface when this is terminated with Al atoms. No differences between these environments have been extracted in the  $f$ -DOS, nor in the  $d$ -DOS between bulk and "below surface" Sm atoms. However, a significant difference has been observed in the  $d_{xy}$  projected part of  $d$ -DOS close to the Fermi level between bulk Sm and Surface Sm atoms (**figure 5b**). The enhancement in the surface  $d_{xy}$  majority DOS close to the Fermi level is consistent with the occurrence of a positively polarized resonant surface state. The question whether this calculated  $d_{xy}$  resonant surface state actually exhibits  $\Lambda_1$  symmetry as observed experimentally is however particularly complex to address, mainly because of the tetragonal symmetry used for the supercell.

These calculations performed for bulk and sub-surface Sm atoms thus strongly support the experimental observations and the assumption that the localized electron pocket around  $\bar{\Gamma}$  is a resonant surface state, likely built on the bulk state close to the Fermi level.

## 5. Conclusion

1  
2  
3 ARPES and SRPES measurements provide the first overview of the surface electronic band structure and  
4 bring important insights in the electronic properties of (111)  $\text{Sm}_{1-x}\text{Gd}_x\text{Al}_2$  epitaxial film. Despite the difficulties  
5 related both to the sharp resonance over a narrow energy range and to the analysis of a complex compound  
6 initially prepared in a different MBE chamber, experimental observations reveal the occurrence of a resonant  
7 surface state. Built on a bulk state, with  $\Lambda_1$  symmetry and  $d$ -character, it appears as a strongly localized electron  
8 pocket around  $\bar{\Gamma}$  in the SBZ. First SRPES measurements show a low temperature positive spin polarization of  
9 this state at the Fermi level. Those results are supported by DOS calculations performed for a supercell taking  
10 the different Sm atoms' environments into account.

11 The observation of a polarized surface state in this unconventional material of interest for spintronic  
12 applications is an important step towards the development of new spintronic devices. Surface/interface  
13 electronic states are namely key parameters to govern transport and magneto-transport properties, as  
14 highlighted in more usual systems. An interesting feature revealed by DOS calculations in this complex  
15 compound is the existence of a surface state, specifically in the case of surface Sm atoms. The accurate control  
16 of the topmost atomic layer, although a challenging task, could be thus an efficient lever to manipulate the  
17 surface state and consequently to tailor magneto-transport properties.

18 In the field of spintronics where surfaces/interface properties always raise interest, we now hope that these  
19 results will motivate further theoretical and experimental work on new devices based on unconventional  
20 magnetic materials.  
21

## 22 23 **Acknowledgment**

24  
25  
26 The authors thank Danielle Pierre for technical help in the sample growth, G. Vasseur for support and fruitful  
27 discussion on the ARPES data analysis. They also acknowledge the synchrotron SOLEIL for provision of  
28 synchrotron radiation facilities and thank the staff for assistance in using the beamline.

29 The project was supported by the Region Lorraine, the Grand Nancy, the Feder, ICEEL, the Agence Nationale  
30 de la Recherche, the French PIA project "Lorraine Université d'Excellence" ANR-15-IDEX-04-LUE."  
31  
32  
33  
34  
35  
36  
37  
38  
39  
40  
41  
42  
43  
44  
45  
46  
47  
48  
49  
50  
51  
52  
53  
54  
55  
56  
57  
58  
59  
60

## References

- [1] A. Fert, A. Barthélémy, and F. Petroff, in *Nanomagnetism Ultrathin Film. Multilayers Nanostructures*, edited by D. L. Mills and J. A. C. Bland, pp. 153–225 (2006).
- [2] K. D. Belashchenko, J. Velev, and E. Y. Tsymlal, *Phys. Rev. B* **72**, 140404(R) (2005).
- [3] J. Moser, M. Zenger, C. Gerl, D. Schuh, R. Meier, P. Chen, G. Bayreuther, W. Wegscheider, D. Weiss, C. H. Lai, R. T. Huang, M. Kosuth, and H. Ebert, *Appl. Phys. Lett.* **89**, 162106 (2006).
- [4] A. N. Chantis, K. D. Belashchenko, E. Y. Tsymlal, and I. V. Sus, *Mod. Phys. Lett. B* **22**, 2529 (2008).
- [5] P. V. Lukashev, J. D. Burton, A. Smogunov, J. P. Velev, and E. Y. Tsymlal, *Phys. Rev. B* **88**, 134430 (2013).
- [6] Y. Wang, P. Deorani, K. Banerjee, N. Koirala, M. Brahlek, S. Oh, and H. Yang, *Phys. Rev. Lett.* **114**, 257202 (2015).
- [7] R. Fetzner, B. Stadtmüller, Y. Ohdaira, H. Naganuma, M. Oogane, Y. Ando, T. Taira, T. Uemura, M. Yamamoto, M. Aeschlimann, and M. Cinchetti, *Sci. Rep.* **5**, 8537 (2015).
- [8] Z.-H. Pan, E. Vescovo, A. V. Fedorov, D. Gardner, Y. S. Lee, S. Chu, G. D. Gu, and T. Valla, *Phys. Rev. Lett.* **106**, 257004 (2011).
- [9] H. Adachi and H. Ino, *Nature* **401**, 148 (1999).
- [10] H. Adachi, H. Kawata, H. Hashimoto, Y. Sato, I. Matsumoto and Y. Tanaka, *Phys. Rev. Lett.* **87**, 127202 (2001).
- [11] J. W. Taylor, J. A. Duffy, A. M. Bebb, M. R. Lees, L. Bouchenoire, S. D. Brown, and M. J. Cooper, *Phys. Rev. B* **66**, 161319(R) (2002).
- [12] S. Qiao, A. Kimura, H. Adachi, K. Iori, K. Miyamoto, T. Xie, H. Namatame, M. Taniguchi, A. Tanaka, T. Muro, S. Imada, and S. Suga, *Phys. Rev. B* **70**, 134418 (2004).
- [13] F. L. Pratt, S. J. Blundell, T. Lancaster, M. L. Brooks, C. A. Steer, and H. Adachi, *Physica B* **374–375**, 34 (2006).
- [14] S. S. Dhesi, G. van der Laan, P. Bencok, N. B. Brookes, R. M. Galéra, and P. Ohresser, *Phys. Rev. B* **82**, 180402(R) (2010).
- [15] T. Chatterji, A. Stunault, and P. J. Brown, *Phys. Rev. B* **97**, 064417 (2018).
- [16] X. H. Chen, K. Q. Wang, P. H. Hor, Y. Y. Xue and C. W. Chu, *Phys. Rev. B* **72**, 054436 (2005).
- [17] Z.H. Wu, J. L. Luo, Z. J. Chen, G. T. Liu, P. Yu and N.L.Wang, *J. Phys. D: Appl. Phys.* **38**, 3567–3571 (2005).
- [18] J.R. Su, C.F. Zhu, B. Wolf and M. Lang, *Journal of Alloys and Compounds* **431**, 45–48 (2007).
- [19] A. Avisou, C. Dufour, K. Dumesnil and D. Pierre, *Journal of Crystal Growth* **297**, 239–246 (2006).
- [20] A. Avisou, C. Dufour and K. Dumesnil, *Journal of Applied Physics* **103**, 07E135 (2008).
- [21] A. Avisou, C. Dufour, K. Dumesnil, A. Rogalev, F. Wilhelm, and E. Snoeck, *J. Phys. Condens. Matter* **20**, 265001 (2008).
- [22] A. Avisou, K. Dumesnil, and C. Dufour, *J. Magn. Magn. Mater.* **316**, 317 (2007).
- [23] M. Da Silva, K. Dumesnil, C. Dufour, M. Hehn, D. Pierre, D. Lacour, F. Montaigne, G. Lengaigne, and S. Robert, *Appl. Phys. Lett.* **98**, 232504 (2011).
- [24] M. Bersweiler, PhD. thesis, University of Lorraine, 2014.
- [25] C. Laubschat, G. Kaindl, W.-D. Schneider, B. Reihl and N. Martensson, *Phys. Rev. B* **33**, 6675 (1986).
- [26] M. Matsunami, T. Hajiri, H. Miyazaki, M. Kosaka, and S. Kimura, *Phys. Rev. B* **87**, 165141 (2013).
- [27] A. Hasegawa and A. Yanase, *J. Phys. F Met. Phys* **10**, 847 (1980).
- [28] A. Hasegawa and A. Yanase, *J. Phys. F Met. Phys* **10**, 2207 (1980).
- [29] V. Kathirvel, S. Chandra, N. V. C. Shekar, and P. C. Sahu, *Physica. B Condens. Matter* **404**, 2130 (2009).
- [30] D. Paudyal, A.K. Pathak, V.K. Pecharsky and K.A. Gschneidner Jr, *J. Phys. Condens. Matter* **25**, 396002 (2013).
- [31] H.J. Gotsis and I. I. Mazin, *Phys. Rev. B* **68**, 224427 (2003).
- [32] M. Bersweiler, K. Dumesnil, F. Wilhelm, and A. Rogalev, *Phys. Rev. B* **88**, 54411 (2013).
- [33] S. Hüfner, *Photoelectron Spectroscopy, Principles and Applications*, Springer-Verlag Berlin Heidelberg, (2003).
- [34] F. Gerken, *J. Phys. F Met. Phys* **13**, 703 (1983).
- [35] E. Guziewicz, B. A. Orłowski, A. Reszka, L. Wachnicki, S. Gieraltowska, M. Godlewski, I. A. Kowalik, B. J. Kowalski, and R. L. Johnson, *Synchrot. Radiat. Nat. Sci.* **2** (2012).
- [36] M. Richter, M. Meyer, M. Pahler, T. Prescher, E. V. Raven, B. Sonntag, and H.-E. Wetzels, *Phys. Rev. A* **40**, 7007 (1989).
- [37] J. Hermanson, *Solid State Commun.* **22**, 9 (1977).
- [38] G. Nicolay, F. Reinert, S. Hüfner and P. Blaha, *Phys. Rev. B* **65**, 033407 (2001).

1  
2  
3  
4  
5  
6  
7  
8  
9  
10  
11  
12  
13  
14  
15  
16  
17  
18  
19  
20  
21  
22  
23  
24  
25  
26  
27  
28  
29  
30  
31  
32  
33  
34  
35  
36  
37  
38  
39  
40  
41  
42  
43  
44  
45  
46  
47  
48  
49  
50  
51  
52  
53  
54  
55  
56  
57  
58  
59  
60

- [39] S. D. Kevan and R. H. Gaylord, Phys. Rev. B **36**, 5809 (1987).
- [40] P. A. Dowben, D. LaGraffe and M. Onellion, J. Phys. Condens. Matter **1**, 6571 (1989).
- [41] R. Wu, C. Li, A. J. Freeman and C.L. Fu, Phys. Rev. B **44**, 9400 (2008).
- [42] D. Li, C.W. Hutchings, P.A. Dowben, C. Hwang, Rong-Tzong Wu, M. Onellion, A.B. Andrews and J.L. Erskine, J. Magn. Magn. Mater. **99**, 85 (1991).
- [43] D. Wegner, A. Bauer, Y. M. Koroteev, G. Bihlmayer, E. V. Chulkov, P. M. Echenique, and G. Kaindl, Phys. Rev. B **73**, 115403 (2006).
- [44] S. C. Wu, H. Li, Y. S. Li, D.Tian, J. Quinn, and F. Jona, Phys. Rev. B **44**, 720 (1991).
- [45] M. Bodenbach, A. Höhr, C. Laubschat, G. Kaindl and M. Methfessel, Phys. Rev. B **50**, 14446 (1994).
- [46] D. Wegner and G. Kaindl, Phys. Rev. B **79**, 140406(R) (2009).

Accepted Manuscript

## Figure captions

**Figure 1.**  $I(E_B, k_{//})$  maps along the high symmetry directions  $\bar{\Gamma}\bar{K}$  and  $\bar{\Gamma}\bar{M}$ . Left: Raw data. Right: Data after normalization to the angle-integrated spectrum; Dotted lines are guides for the eyes. Measurements were performed at 5K, for a photon energy of 32 eV and a p-polarization.

**Figure 2.** (a) Energy dispersion curves along  $k_{//}$  for the different contributions identified in Figure 1 (open circles). The dot red curves are parabolic fits using the free electron model approximation. The extracted values of  $m^*$  and  $E_0$  are given next to the curves ( $m^*/E_0$ ). (b) and (c) Iso-energy ( $k_x, k_y$ ) maps for different binding energies across the various contributions identified in (a). Measurements were performed at 5K for an incident p-polarized photon beam of 32 eV.

**Figure 3.** (a) Bulk BZ of SGA in which  $k_z$  corresponds to the [111] direction of the fcc BZ. The blue and red areas correspond to the measured areas presented on the right (b) and (c) Fermi surface mapping in the ( $k_z, k_y$ ) and ( $k_x, k_y$ ) planes (measured at 5K with a p-polarized photon beam).

**Figure 4.** (a) Angle-integrated EDC curves around the  $\bar{\Gamma}$  point after subtraction of the divalent contributions for p- (green circles) and s-(black squares) polarization. Measurements were performed at 5K and for a photon energy of 32 eV. The red curves correspond to the fits using three Lorentzians multiplied by the Fermi function. (b) Perpendicular to the plane spin polarization measured at 30K ( $h\nu = 32$  eV, p-polarized photon beam).

**Figure 5.** Electronic structure calculations performed in LSDA+U+SO (Wien2k code): (a) Band structure for bulk  $\text{SmAl}_2$ . The color dots are guides for the eyes. (b) Density of states projected on  $d_{xy}$  orbitals for Sm atoms located in the core of the layer (black) and at the surface (red).

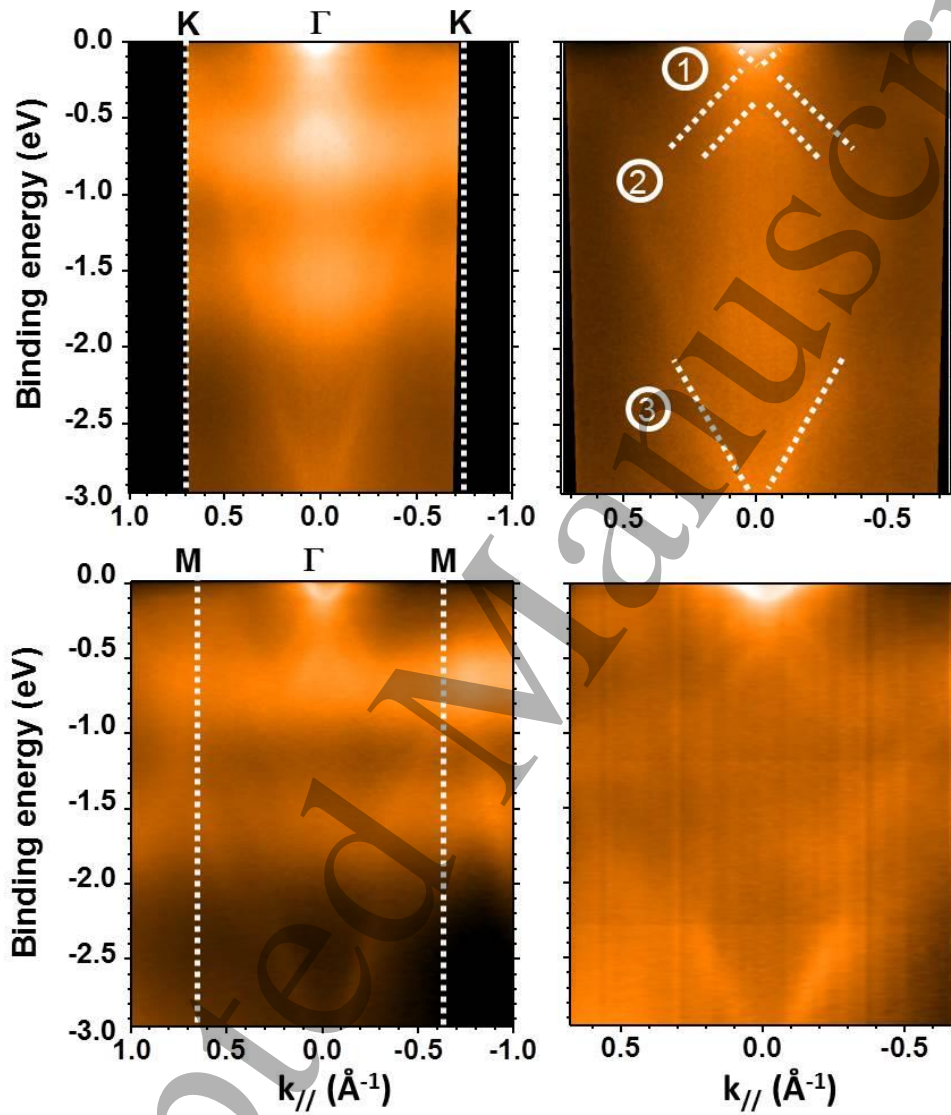


Figure 1. (Color online)

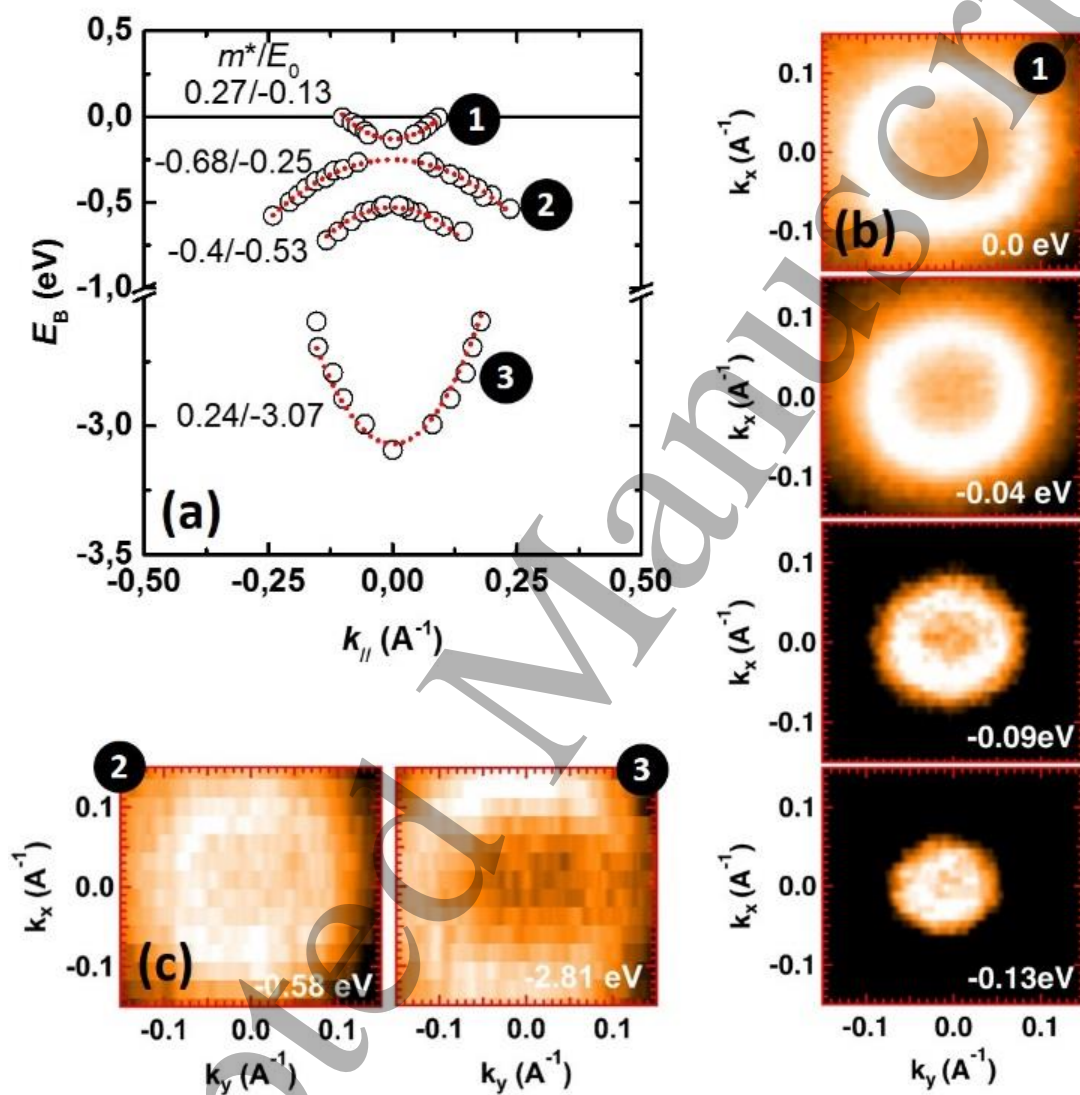
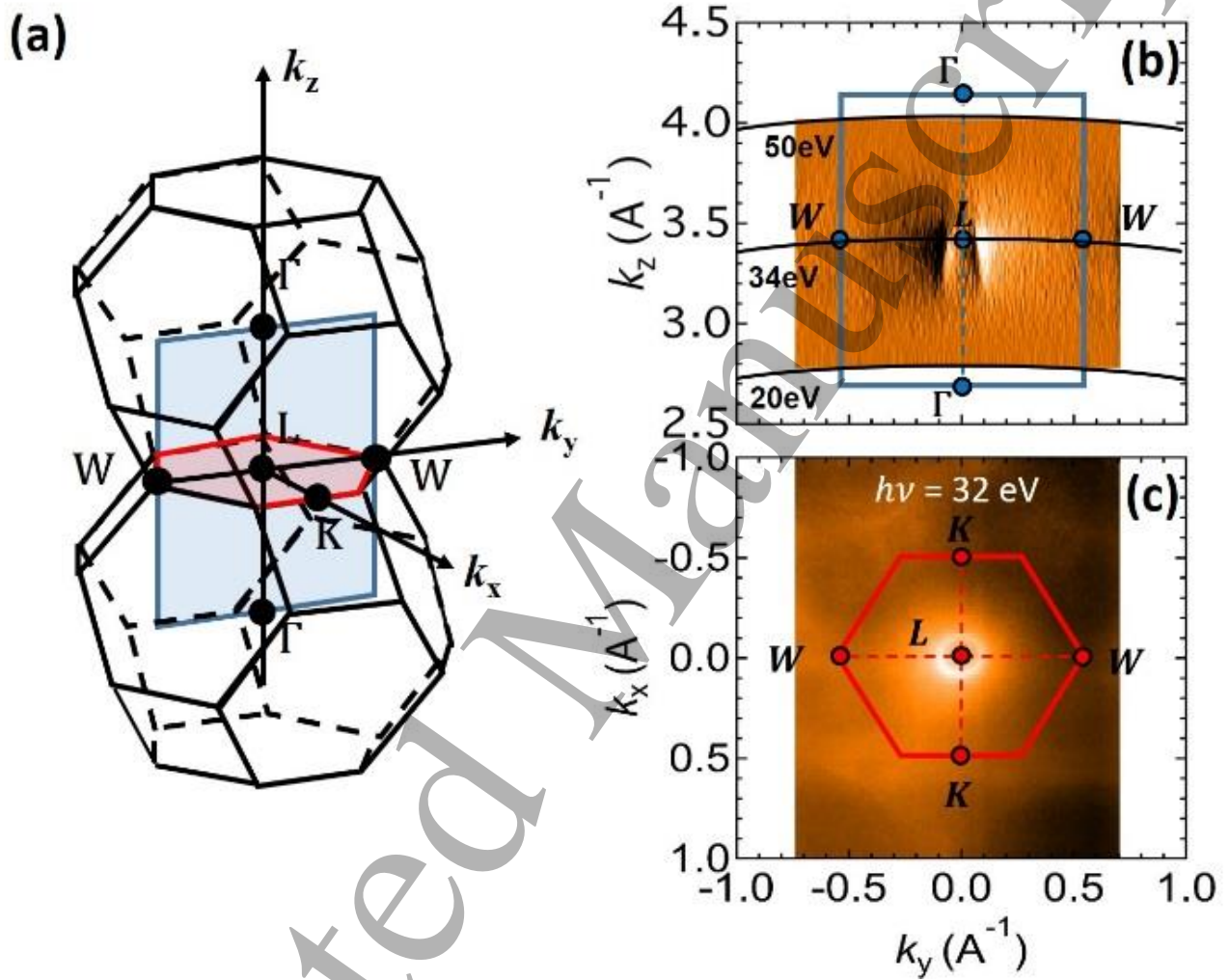
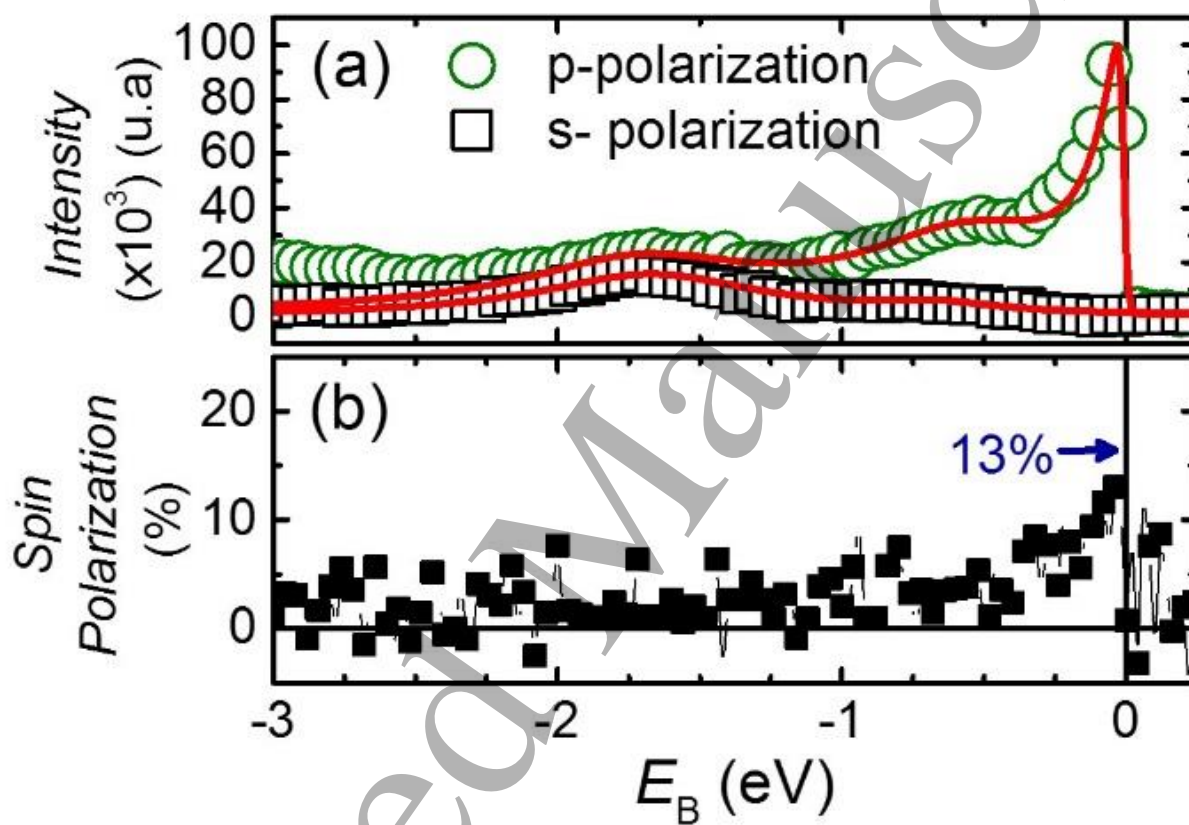


Figure 2. (Color online)



**Figure 3.** (Color online)



**Figure 4.** (Color online)

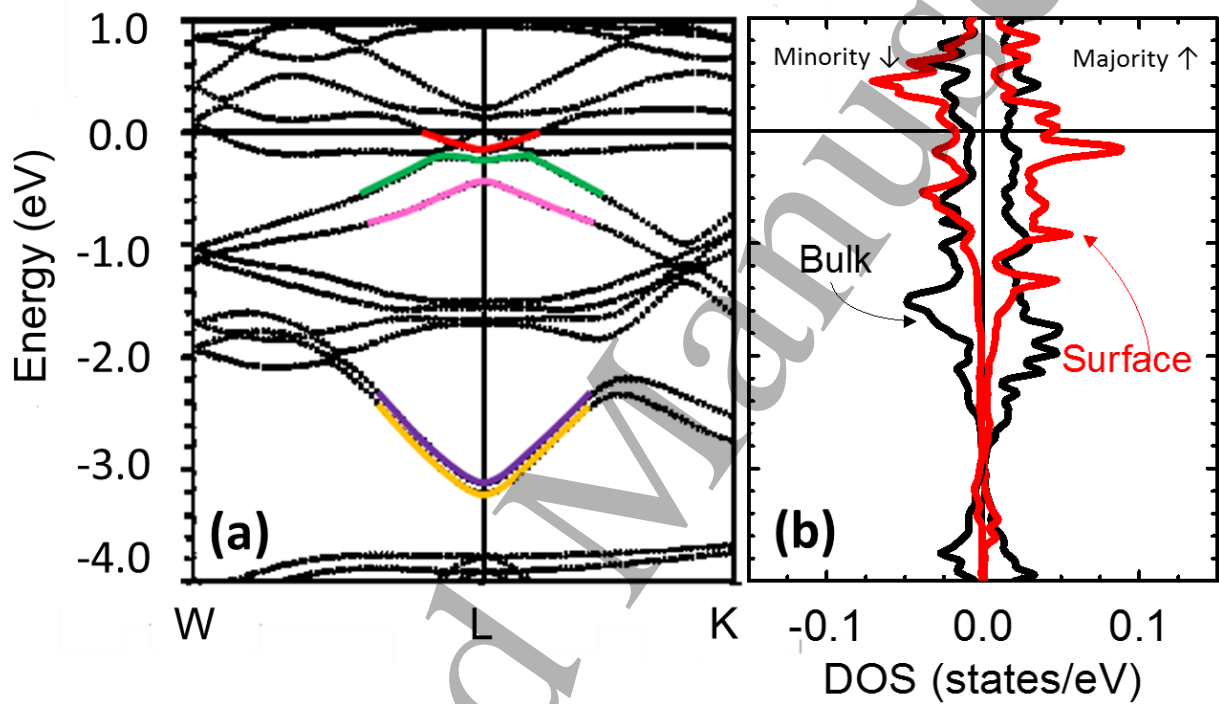


**Figure 5.** (Color online)